Hybrid M13 bacteriophage-based vaccine platform for personalized cancer immunotherapy

Xue Dong [a,1], Pei Pan [b,1], Jing-Jie Ye [b], Qiu-Ling Zhang [b], Xian-Zheng Zhang [a,b,*]

[a] *Institute for Advanced Studies, Wuhan University, Wuhan 430072, PR China*
[b] *Key Laboratory of Biomedical Polymers of Ministry of Education & Department of Chemistry, Wuhan University, Wuhan 430072, PR China*

ARTICLE INFO

ABSTRACT

Although cancer vaccines exhibit great advances in the field of immunotherapy, developing an efficient vaccine platform for personalized tumor immunotherapy is still a major challenge. Here we demonstrate that a bioactive vaccine platform (HMP@Ag) fabricated with hybrid M13 phage and personal tumor antigens can facilitate delivery of antigens into lymph nodes and activate antigen-presenting cells (APCs) through the Toll-like receptor 9 (TLR9) signaling pathway, which boosts both innate and adaptive immune response. As an adjuvant platform, hybrid M13 phages can deliver various tumor-specific antigens through simple adsorption to support the current development of personalized vaccines for cancers. Notably, the HMP@Ag vaccine not only prevented the tumors, but also delayed the tumor growth in established (subcutaneous and orthotopic) and metastatic tumor-bearing models while synergy with immune checkpoint blockade (ICB) therapy. Moreover, HMP@Ag triggered a robust neoantigen-based specific immune response in tumor-specific mutation models. In a clinically relevant surgery model, using autologous cell membrane from primary tumors-based HMP@Ag cooperation with ICB dramatically inhibited the post-operation recurrence, and elicited a long-term immune memory effect simultaneously. These findings imply that the M13 phage represents a powerful tool to develop a bio-activated hybrid platform for personalized therapy.

1. Introduction

Immunotherapy has emerged as powerful therapeutic in the clinic for cancer treatment by training the host immune system to attack tumor cells [1–5]. Among various types of immune-based strategies, the cancer vaccine as an immunomodulator can activate the specific anti-tumor immune response and form a long-term memory effect to destroy tumor cells [6–9]. Recent developments in cancer vaccines have led to a renewed interest in constructing nano-vaccines based on nanotechnology [10–15]. For instance, utilizing nano-vehicle was proved to realize antigen and adjuvant co-loading [16,17]. Moreover, it was reported that the cancer vaccine could target lymph nodes (LNs) by bio-orthogonal chemistry strategies [18]. Despite these considerable advances, the design of vaccines with potent immune-stimulating effects remains a major challenge, especially in those personalized cancer vaccine platforms [19,20].

Natural microorganisms with pathogen-associated molecular patterns (PAMPs) can effectively robust the host's innate immune response compared with those vaccines based on synthetic materials [21–25]. The first bacteria-based vaccine was developed by the injection of heat-inactivated Streptococcus pyogenes and *Serratia marcescens* bacteria to treat tumors, known as Coley's toxins [26]. More recently, a large number of studies have revealed that multiple cancer treatments based on microorganisms, including bacterial, viruses and microbial bioactive components could elicit a strong immune response [27–30]. However, the biosafety of these pathogen-based vaccines is still a key issue. For example, the virulence and pathogenicity of bacteria might induce immune-related adverse events, which greatly limits their clinical application [31].

Bacteriophages regarded as a kind of prokaryotic virus, are mainly composed of nucleic acid and capsid protein. It was demonstrated that bacteriophages possessed a higher safety profile on account of only specifically infection bacteria but not eukaryotic cells [32]. M13 phages are classified as filamentous phages, which can directly activate the toll-like receptors (TLR) pathway to further mediate the awakening of adaptive immune responses due to the abundance

---
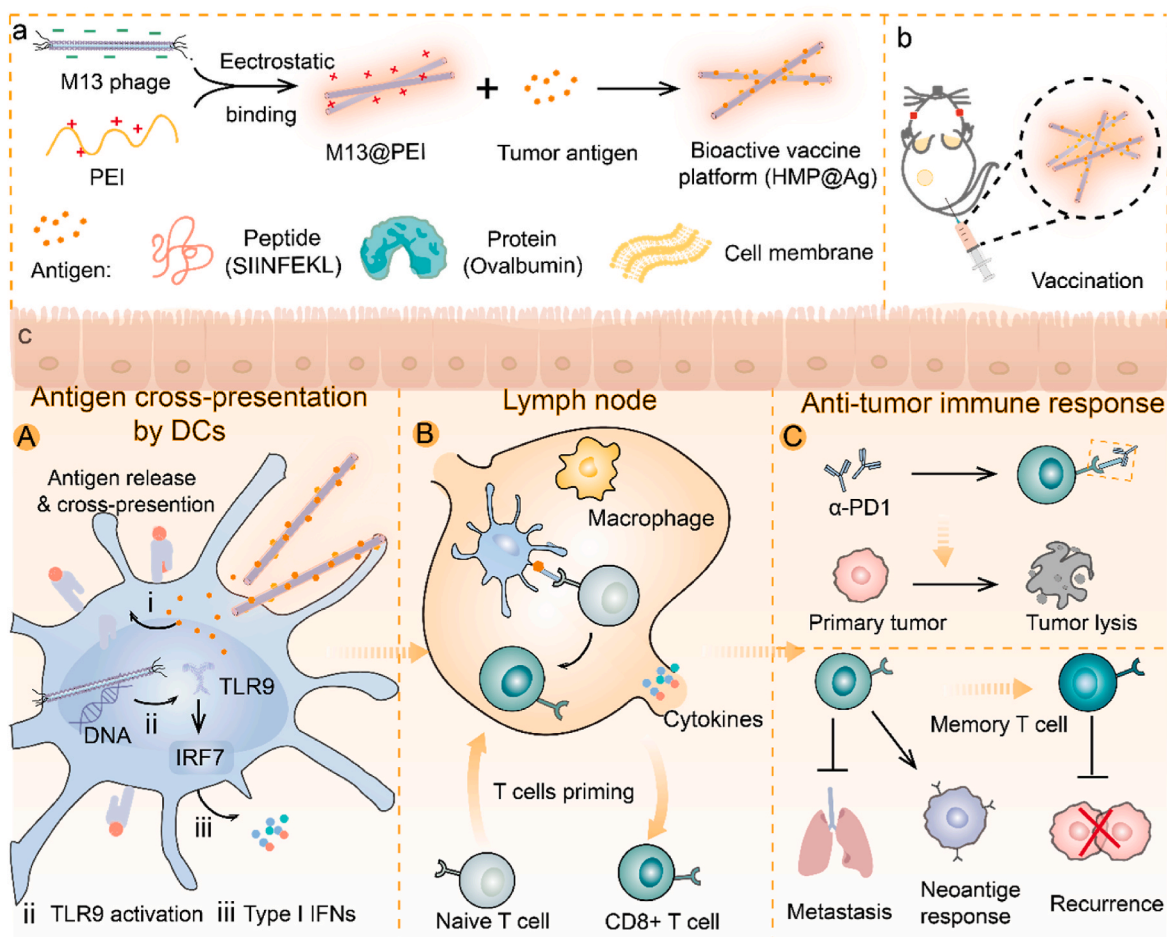
Fig. 1. Schematic illustration for the M13 phage-based vaccine platform. (a) Construction of the tumor antigen-loaded hybrid vaccine by M13 phage. (b–c) Schematic of demonstration the HMP@Ag vaccine for boosting potent anti-tumor immune response. After mice subcutaneous vaccination, HMP@Ag vaccine was first internalized by DCs for antigen release and cross-presentation to promote DCs maturation (A). Then, mature DCs migrated to lymph node for further activation and expansion of antigen-specific CD8$^+$ T cells (B). Such M13 phage-based vaccine combination with ICB treatment could inhibit primary and metastatic cancers, trigger the neoantigen-based CTL response, and represented remarkable tumor recurrence suppression effect after surgery (C).

deoxycytidylate-phosphate-deoxy guanylate (CpG) regions in their genomes [33,34]. Additionally, with intrinsic pathogen characteristics, M13 phages can be quickly recognized by antigen-presenting cells (APCs) to boost innate immunity [35,36]. Owing to their high immunogenicity and safety, as well as excellent stability and ease of storage, M13 phages are promising candidates for the development of powerful vaccine platforms. A general M13 phage-based vaccine was engineered to express certain antigen peptides by using phage display technology [37,38]. Whereas, the displayed target molecule was restricted by various factors (e.g., length of the sequence, antigen conformation) [39]. Therefore, it is necessary to develop a simple tactic to prepare phage-based vaccine platform. With the unique rod-like structure and abundant chemical modification sites, phages are excellent biological building blocks to conjugate multifunctional nanomaterials for biomedical applications [40–43].

In this study, we established a hybrid M13 phage vaccine platform to co-present tumor-specific antigens for initiating innate and adaptive immune responses. Literature studies showed that M13 phages were negatively charged on the surface, which made them more likely to adsorb positively charged materials. Meanwhile, polyethyleneimine (PEI) as a cationic polymer was widely employed in gene and protein delivery [44]. Here, a phage-based vaccine platform was prepared by simply mixing M13 phages and PEI. M13 phages were coated with PEI driven by electrostatic force to form a hybrid phage complex (M13@PEI). Subsequently, antigen pool (Ag) including peptides,

proteins and tumor-derived cell membranes (CM) were adsorbed onto M13@PEI to fabricate an active hybrid M13 phage-based vaccine platform (HMP@Ag) (Fig. 1a). When the mice were vaccinated subcutaneously, such a hybrid M13 phage carrier could promote antigen delivery and cross-presentation effectively. After the APCs mature in lymph nodes (LNs), the naïve T cells were recruited and further activated toward cytotoxic CD8$^+$ T cells (Fig. 1b and c). Profiting from the superiority of the M13 phage, such HMP@Ag vaccines combination with immune checkpoint blockade (ICB) could trigger a robust specific anti-tumor immune response in multiple tumor-bearing models.

2. Materials and methods

2.1. Materials

M13 phages were provide from Wuhan GeneCreate Biological Engineering Co., Ltd. Polyethylenimine (PEI) with a molecular weight of 25 kDa, OVA were purchased from Sigma-Aldrich. GM-CSF, IL-4, Membrane and cytosol protein extraction kit, D-luciferin potassium salt, Hoechst 33,342 and cell counting kit-8 (CCK-8) were purchased from Beyotime Biotechnology Co. Ltd. Lyso Tracker Red, collagenase IV, hyaluronidase and DNase I were purchased from Yeasen Biotechnology Co., Ltd. ELISA kits for IL-6, TNF-α, IL12p40, IFN-β, IgG and IFN-γ were supplied by 4 A Biotech Co., Ltd. OVA257-264 peptide was bought from Shanghai Dechi Biosciences Co., Ltd. α-PD1 was purchased from

Bioxcell. PE-*anti*-mouse CD3 (clone 17A2), FITC anti-mouse CD4 (clone GK1.5), APC anti-mouse CD8a (clone 53-6.7), PE anti-mouse CD11c (clone N418), FITC anti-mouse CD80 (clone 16-10A1), APC anti-mouse CD86 (clone GL-1), PE anti-mouse CD11b (clone M1/70), APC anti-mouse CD11b (clone M1/70), PE anti-mouse F4/80 (clone BM8), FITC anti-mouse TLR9 (clone S18025A), APC anti-mouse CD40 (clone 3/23), APC anti-mouse H-2Kb bound to SIINFEKL (clone 25-D1.16), FITC anti-mouse CD8a (clone 53-6.7), PE anti-mouse CD44 (clone IM7), APC anti-mouse CD62L (clone MEL-14), Alexa Fluor® 647 anti-mouse I-A/I-E (clone M5/114.15.2), FITC anti-mouse H-2Kd/H-2Dd (clone 34-1-2S), PE Streptavidin and Flex-T™ Biotin H-2 K(b) OVA Monomer (SIIN-FEKL) anti-bodies were all provided from BioLegend.

2.2. Cell lines and animal models

B16-OVA cells, RAW 264.7 cells, CT26 cells and 4T1 cells were bought from China Center for Type Culture Collection (CCTCC). BMDCs and lymphocytes isolation protocols were referred to the previous studies [36]. In brief, BMDCs were separated from femur bones of 6-week-old C57BL/6 mice. Then, cells were differentiated with 10 ng mL^{-1} IL-4 and 20 ng mL^{-1} GM-CSF in RPMI 1640 culture medium for 6 days for further studies. Lymphocytes were isolated from spleen of 6-week-old C57BL/6 mice and cultured in DMEM medium.

All animal studies were approved by the Institutional Animal Care and Use Committee (IACUC) of the Animal Experiment Center of Wuhan University (Wuhan, China), performed on animal accreditation number WP20210513. All experimental procedures were performed following the Regulations for the Administration of Affairs Concerning Experimental Animals approved by the State Council of People's Republic of China. All animals were anaesthetized by isoflurane and sacrificed by CO$_2$-euthanasia. To construct subcutaneous tumor bearing model for therapy, tumor cells of B16-OVA (3×10^5 cells per mice), CT26^{neo} (5×10^5 cells per mice) and 4T1^{neo} (5×10^5 cells per mice) were subcutaneously injected into the 6-week-old female C57BL/6 mice and BALB/c mice severally. For the prophylactic study, B16-OVA cells (3×10^5 cells per mice) were subcutaneously injected into the female C57BL/6 mice after vaccination. For the establishment the orthotopic breast cancer model, 4T1-luc (1×10^6 cells per mice) were injected in left breast pad of BALB/c mice.

2.3. Preparation and characterization of hybrid M13 phage

1×10^{11} PFU mL^{-1} M13 phages were dispersed in ultrapure water and 10 µL PEI (1 mg mL^{-1}) was then added to the phages solution. After a gentle mixture, the complex was incubated for 15 min at room temperature to obtain hybrid phages (M13@PEI). The excess PEI was removed by ultrafiltration (MWCO: 100 kDa). The prepared M13@PEI was mixed with OVA (10 µg mL^{-1}) for another 30 min at 37 °C to form a hybrid phages-based vaccine platform (noted as MPO, "M" was M13 phage; "MP" was a hybrid phage complex of M13@PEI; "MPO" was M13@PEI loaded with OVA). For characterization of hybrid phages, the zeta potentials of M13 phages, M13@PEI and MPO were measured with a Zetasizer (Nano ZS, Malvern Instruments). The morphology of M13 phages and M13@PEI were observed by TEM (JEOL 2000FX instrument).

To investigate the stability of the MPO vaccine, M13 phage and MPO were dispersed in three biological solutions (PBS, 1640 culture medium and serum) at 4 °C for one week. Then, the zeta potentials in PBS were detected every 24 h. Also, images of M13 phage and MPO in different solutions were recorded every other day.

2.4. In vitro immune stimulation effects of hybrid phages on APCs

To assess the level of DCs maturation, BMDCs were seeded in a 12-well plate with a density of 4×10^5 cells per well. OVA (10 µg mL^{-1}), M13 phages (1×10^{11} PFU mL^{-1}), M13@PEI (1×10^{11} PFU mL^{-1} of phage and 10 µg mL^{-1} PEI) and MPO (1×10^{11} PFU mL^{-1} of phage, 10 µg mL^{-1} PEI and 10 µg mL^{-1} OVA) were co-cultured with BMDCs for 24 h. Then, cells were collected and stained with fluorescence labeled specific antibodies of CD11c, CD80, CD86 and CD40. FCM was used to analyze the expression of these cell surface markers. Meanwhile, the supernatant was used for cytokines measurement of TNF-α, IFN-α, IL12p40 and IL-6 by enzyme-linked immunosorbent assay (ELISA) assay.

For macrophages activation assay, RAW 264.7 cells were seeded in a 12-well plate with a density of 4×10^5 cells per well. OVA, M13 phages, M13@PEI and MPO with the same concentration as in the aforementioned experiment were incubated with macrophages. After 24 h, cells were harvested and stained fluorescence-labeled specific antibodies of CD11b, CD86 for FCM analysis. The supernatant was collected for IFN-β detection by using ELISA kit.

2.5. In vitro OVA antigen presentation assessment

To evaluate the antigen presentation ability of DCs, BMDCs were seeded in a 12-well plate with a density of 4×10^5 cells per well. OVA (10 µg mL^{-1}) and MPO (1×10^{11} PFU mL^{-1} of phage, 10 µg mL^{-1} PEI and 10 µg mL^{-1} OVA) were added and incubated for 24 h. DC cells were then stained with APC anti-mouse H-2Kb bound to SIINFEKL antibodies to confirm the efficiency of OVA antigen presentation by DC. Besides, BMDCs were also treated with PBS, OVA, M13, M13@PEI and MPO and further analyzed the expression of MHCI and MHCII.

2.6. In vitro cell uptake of antigen

BMDCs (4×10^5 cells) were seeded in a 12-well plate and then treated with OVA (10 µg mL^{-1}) as well as MPO (1×10^{11} PFU mL^{-1} of phage, 10 µg mL^{-1} PEI and 10 µg mL^{-1} OVA) for 24 h (OVA labeled with Cy5). After that, cells were harvested and stained with CD11c for quantitative analyzing the intracellular fluorescence intensity of Cy5 by FCM.

For visualization the distribution of antigen in DCs, BMDCs (4×10^5 cells) were seeded in glass-bottomed culture dish and Cy5-labeled OVA (10 µg mL^{-1}) and MPO (1×10^{11} PFU mL^{-1} of phage, 10 µg mL^{-1} PEI and 10 µg mL^{-1} OVA) were added for 6 h and 24 h incubation. Then, the cell nucleus and lysosomes were stained by Hoechst33342 and Lyso-Tracker Green severally. The fluorescence co-localization was observed with super-resolution fluorescence microscopy.

2.7. M13 phages mediated lymphocyte proliferation and cytotoxic T lymphocyte (CTL) priming assays

BMDCs (4×10^5 cells) were seeded in a 12-well plate and pre-stimulated with OVA$_{257-264}$ peptide (10 µg mL^{-1}), M13 phages (1×10^{11} PFU mL^{-1}), M13@PEI (1×10^{11} PFU mL^{-1} of phage and 10 µg mL^{-1} PEI) and MPO (1×10^{11} PFU mL^{-1} of phage, 10 µg mL^{-1} PEI and 10 µg mL^{-1} OVA$_{257-264}$ peptides) for 24 h. After cocultivation, mature DCs were harvested by centrifugation (500 g, 5 min). For lymphocyte proliferation, the spleen cells were isolated from the spleen of C57BL/6 mice. Then, the spleen lymphocytes were labeled with carboxy-fluorescein diacetate, succinimidyl ester (CFSE) probe by using CFDA SE Cell Proliferation Assay and Tracking Kit to track lymphocytes. Per-treated DCs were co-cultured with CFSE-marked lymphocytes at a ratio of 1:5 (DCs: lymphocytes) for another 72 h. Cells were collected and stained with APC anti-mouse CD8a antibody for FCM analysis proliferation capacity of CD8$^+$ T cells.

For the CTL-mediated cytotoxicity assay, BMDCs were pre-treated with the same concentration as in the aforementioned experiment of OVA$_{257-264}$ peptide, M13 phages, M13@PEI and MPO to obtain mature DCs. Mature DCs were then co-incubated with spleen lymphocytes at a ratio of 1:5 (DCs: lymphocytes) for 24 h. Subsequently, activated spleen lymphocytes were harvested and cultured with B16-OVA cells in a 24-
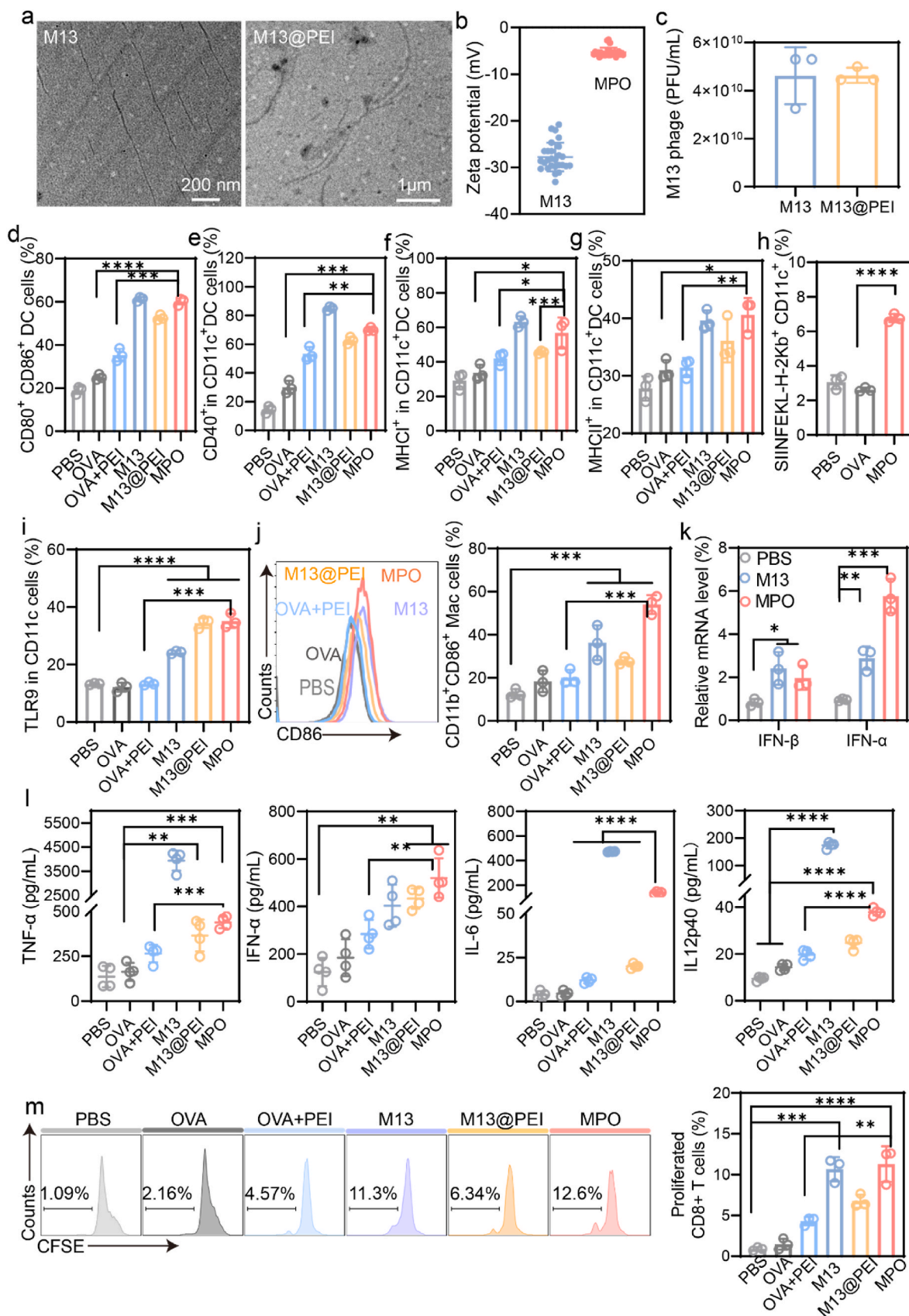
(caption on next page)

Fig. 2. Characterization and APCs activation of hybrid phage vaccine *in vitro*. (a) TEM image of the M13 phage (left) and M13@PEI (right). The length of the M13 phage was about 900 nm. (b) Zeta potential of M13 phage and MPO after storage at 4 °C for one week (n = 3). (c) Bioactivity of the M13 phage after electrostatic self-assembly of cationic polymer PEI (n = 3). (d–e) The expression of CD80$^+$ CD86$^+$ and CD40 in BMDCs with various treatments for DC mature evaluation (n = 3). (f–h) Antigen presentation of MHCI, MHCII and OVA cross-presentation efficiencies in BMDCs after treatment with OVA, OVA + PEI, M13, M13@PEI and MPO for 24 h (n = 3). (i) TLR9 activation in BMDCs after a 24 h incubation with indicated formulations (n = 3). (j) Representative FCM image (left) and corresponding quantification (right) of RAW 264.7 macrophages activation after different treatments for innate immune analysis (n = 3). (k) Transcript abundance of IFN-β and IFN-α in RAW 264.7 Macs and BMDCs with MPO treatment (n = 3). (l) The cytokines secretion in the culture medium of BMDCs after different treatments (n = 4). (m) Typical FCM image (left) and statistical data (right) showing splenic CD8$^+$ T cells proliferation (labeled with CFSE) after various treatments for 72 h (n = 3). Significance between every two groups was calculated using unpaired two-tailed Student's *t*-test. The mean values and S.D. are presented. *P < 0.05, **P < 0.01, ***P < 0.001, ****P < 0.0001.

well plate with an effective target cell ratio of 10:1. After another 24 h incubation, the supernatant was collected to detect the LDH content with LDH Cytotoxicity Assay Kit. Additionally, IFN-γ secreted by cytotoxicity T cells was examined by ELISA assay.

2.8. In vivo dLNs accumulation analysis

In brief, OVA was labeled with Cy5 first. Then, OVA and MPO were subcutaneously injected into the female C57BL/6 mice at the tail base. After 24 h, the draining lymph node was isolated for *ex vivo* fluorescence imaging. In addition, the dLNs were digested to prepare single-cell suspension and stained PE anti-mouse CD11c antibody for analysis *in vivo* OVA antigen uptake by DCs.

2.9. Immune responses in the dLNs

B16-OVA (3×10^5 cells per mice) were subcutaneously injected into the female C57BL/6 mice. Seven days after first immunization with PBS, OVA$_{257-264}$ peptide, M13@PEI and MPO, the draining lymph node was harvested and grinded by 2% FBS buffer solution to obtain cell suspension. Then, the cell samples were stained with various antibodies for FCM analysis. For mature DCs analysis, cells were stained with PE anti-mouse CD11c, FITC anti-mouse CD80, APC anti-mouse CD86 and APC anti-mouse CD40 antibodies. To evaluate the antigen presentation, cell samples were marked by PE anti-mouse CD11c and APC anti-mouse H-2Kb bound to SIINFEKL. The activated macrophages were tagged with PE anti-mouse F4/80, APC anti-mouse CD11b, PE anti-mouse CD11b, and APC anti-mouse CD86 antibodies. For SIINFEKL-specific CD8$^+$ T cells evaluation, PBMCs were collected after various treatments and stained with PE Streptavidin and Flex-T™ Biotin H-2 K(b) OVA Monomer (SIINFEKL) following the standard protocol of the tetramer staining assay. Cytokines in mouse serum of IgG, IFN-γ, TNF-α, IL-6, IFN-α and IFN-β were also measured by ELISA assays.

2.10. OVA-based phage vaccine for prophylactic and therapeutic studies

For prophylactic assay *in vivo*, 6-week-old female C57BL/6 mice were divided into five groups randomly. Mice received PBS, OVA$_{257-264}$ peptide, M13, M13@PEI and MPO by injection at the tail base subcutaneously for every other week altogether three times. Seven days after the last immunization, B16-OVA cells were implanted subcutaneously into the right flank of mice for tumor challenge. The body weight and tumor growth were recorded once every other day. The tumor volume was calculated as $V = 0.5 \times L \times W^2$, in which L and W are the longest and the shortest lengths of the tumor, respectively.

To evaluate the therapeutic effect of phage vaccines, ICB was used for synergy vaccine therapy. B16-OVA cells were injected subcutaneously at the right flank of mice. After five days, mice were divided into six groups blindly and immunized PBS, OVA$_{257-264}$ peptide, M13, M13@PEI, MPO and MPO + α-PD1 (25 μg per mice, *i. v.*) respectively. The body weight and tumor growth were monitored once every other day.

For the anti-metastasis study, C57BL/6 mice were intravenously injected B16-OVA cells with a density of 1×10^5 cells per mice. 24 h later, mice were treated with PBS, OVA$_{257-264}$ peptide, M13, M13@PEI,

MPO and MPO + α-PD1. The mice were sacrificed after 16 days and lung tissues were harvested for observation distant metastasis with H&E staining.

### 2.11. MPM-based vaccine platform for personalized therapy

The hybrid phage (M13@PEI)-loaded with the antigen based on the tumor cell membrane (Mem) was signified as MPM. To establish the neoantigen phage vaccines, the cell membranes of neoantigen cell lines were extracted as tumor-specific antigens by using membrane and cytosol protein extraction kit. For personalized therapeutics studies, subcutaneous colon cancer and breast cancer models were primarily constructed by injection tumor cells (CT26^{neo} and 4T1^{neo}) at the right flank of the BALB/c mice. Four days after inoculation of tumors, mice were divided into six groups randomly and immunized with PBS, Mem, M13, M13@PEI, MPM and MPM + α-PD1 severally. Mice were immunized on day 4, 10, 16 and injected α-PD1 on day 6, 8, 12, 14, 18 and 20. The body weight and tumor growth were monitored once every other day.

For orthotopic breast cancer model establishment, 4T1-luc cells were inoculated at the left breast pad of BALB/c mice. After seven days (denote as day 0), mice were treated with various vaccines with PBS, Mem, M13, M13@PEI, MPM and MPM + α-PD1 (vaccines inoculation every seven days for total two times, α-PD1 injection twice every seven days amount to four times). The tumor progression was monitored by the IVIS imaging system to observe the bioluminescence of tumor cells once a week.

To construct subcutaneous surgical resection model in breast cancers, 4T1–luc cells were transplanted in BALB/c mice. Seven days after the tumor inoculation, the tumor tissues were excised surgically and collected for personalized vaccines preparation. The tumor tissues were digested with 1 mg mL^{-1} collagenase IV, 0.2 mg mL^{-1} hyaluronidase and 0.1 mg mL^{-1} DNase I for 2 h at 37 °C. The cell suspension was filtered through a 70 μm nylon cell strainer and centrifuged to obtain cells. After lysis of red blood cells (RBCs), tumor cells were obtained and then extracted cell membranes through membrane protein extraction kit. Personalized cell membrane phage vaccines derived from tumor-bearing mice were prepared with the above-mentioned method. Four days after the surgery, mice were randomly assigned to six groups and accepted vaccines with PBS, Mem, M13, M13@PEI, MPM and MPM + α-PD1 treatments every seven days for total of two times. The recurrence of the tumor was detected by the bioluminescence of tumor cells every week.

2.12. Statistical analysis

The experimental data were presented with average values, expressed as means ± SD. Statistical analysis was conducted by using Student's t-test to compare the two groups, and multiple comparisons were used one-way analysis of variance (ANOVA).
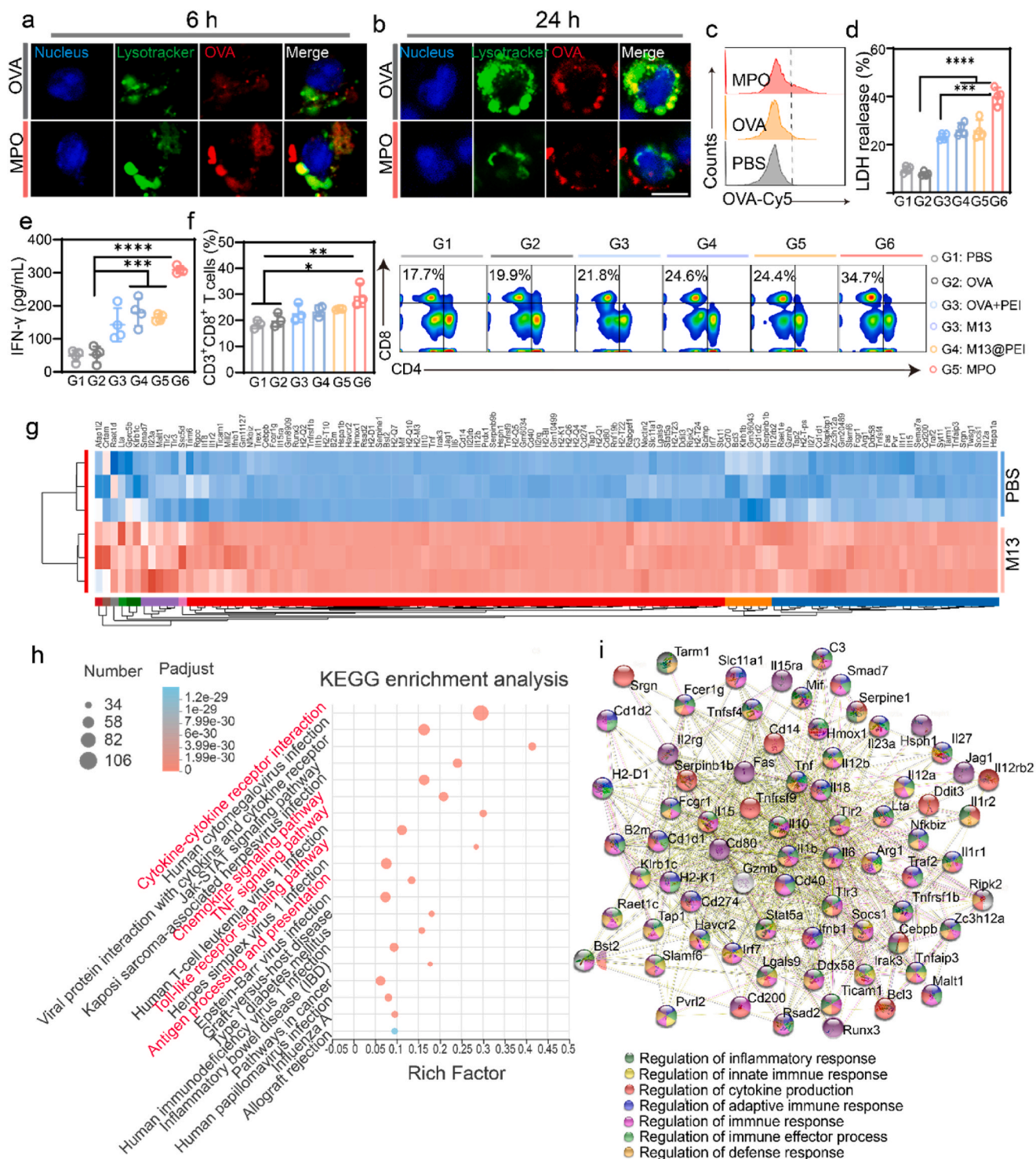
Fig. 3. The stimulation of CTL response and transcriptome analysis *in vitro*. (a–b) Super-resolution focal fluorescence images of BMDCs after uptake of antigen after incubation with OVA and MPO for 6 h in a and 24 h in b. The nuclei and lysosomes were stained with Hoechst 33342 (blue) and LysoTracker Green (green), respectively. OVA was labeled by Cy5 (red) (Scare bar: 10 μm). (c) Representative FCM image of OVA fluorescence intensity in BMDCs after treatment with OVA and MPO for 24 h. (d) Activated lymphocytes-mediated cytotoxicity toward B16-OVA tumor cells. The effector/target ratio was 10:1. Spleen lymphocytes were pre-treated with mature DCs (with various treatments for 24 h) for 24 h (n = 4). (e) IFN-γ level secreted by cytotoxic T lymphocyte in the culture medium after co-incubation with pre-treated DCs and splenocytes for 24 h (n = 4). (f) The corresponding quantification (right) and typical FCM image (left) of CD8+ T cells activation with the same treatments as in panels d (n = 3). (g) Heat map of significantly upregulation genes of BMDCs after M13 phage treatment (fold change ≥2 and p < 0.05 (n = 3). (h) KEGG enrichment for pathway analysis involved in the immune process affected by M13 phage treatment. (i) The functional interaction network of related genes in M13 phage stimulating the immune system. The analysis was used the search tool for the retrieval of interacting genes/proteins (STRING) algorithm. Significance between every two groups was calculated using unpaired two-tailed Student's *t*-test and multiple comparisons were used one-way analysis of variance (ANOVA). The mean values and S.D. are presented. *P < 0.05, **P < 0.01, ***P < 0.001, ****P < 0.0001. (For interpretation of the references to color in this figure legend, the reader is referred to the Web version of this article.)

3. Results and discussion

3.1. M13 phage vaccine-mediated APCs activation in vitro

We first fabricated an M13 phage platform for antigen adsorption. A positively charged cationic polymer PEI (with a molecular mass of 25K) was deposited on the negatively charged M13 phage *via* electrostatic self-assembly with the different mass ratio of M13 phage and PEI to form a hybrid phage-based platform (M13@PEI). The zeta potential of M13@PEI was 28 mV at 10 μg mL^{-1} of PEI, suggesting the negatively charged antigen could adsorb through the electrostatic interaction with high efficiency (Supplementary Fig. S1a). Next, we investigated the immune stimulation effects and cytotoxicity of phage-based vaccines on APCs *in vitro*. As shown in Supplementary Figs. S1b–d the cytotoxicity of the MPO vaccine increased with the higher concentration of PEI, and the proportion of mature DC decreased accordingly. The obtained M13@PEI was incubated with ovalbumin (OVA) at a mass ratio of 1:1 (w/w) [44] for another 30 min to construct the MPO vaccine. The zeta potential of the M13 phage was about −26.7 mV, indicating a negatively charged virus certainly. The MPO vaccine showed decreased zeta potential from 28 mV to −5.3 mV compared to M13@PEI, indicating the antigen adsorption successfully (Supplementary Fig. S1e). And the adhesion efficiency of OVA was about 97.3%. Besides, compared with day 0, MPO and M13 phage showed satisfactory stability with minimal changes in zeta potentials after being stored in PBS at 4 °C for 7 days (Fig. 2b). The images and TEM picture after 7 days of storage in biological solutions also confirmed the stability of M13 phage-based vaccine (Supplementary Fig. S2a-b). All these results suggested that the antigen was loaded successfully with high efficiency and stability. For the natural liveness evaluation of M13 phage, a double agar layer method showed that the plaque-forming unit (PFU) of M13 phage was hardly changed after coating with PEI (Fig. 2c and Supplementary Fig. S3).

The APCs maturation induced by the M13 phage was then examined. After co-incubation of BMDCs with OVA, OVA + PEI, M13 phage, M13@PEI and MPO for 24 h, the expression of co-stimulatory markers was analyzed by flow cytometer (FCM) (Fig. 2d and e and Supplementary Figs. S4a–b). The OVA + PEI treated group induced a slight upregulation in the co-stimulatory molecule compared with the free OVA treated group. However, BMDCs with M13 phage and MPO treatments showed the highest up-regulation of maturation markers (CD80, CD86 and CD40 in CD11c^{+} cells) due to the potent immunogenicity of M13phages. Notably, there was no significant difference in the expression of these molecules between the groups treated with M13 phage or MPO, further indicating that M13 phage could effectively robust the activation of BMDCs. On account of the important role of antigen presentation efficiency in initiating subsequent immune responses [45], the presentation of OVA on DCs was investigated. Stimulating BMDCs by M13 phage and MPO resulted in an increased proportion of MCHI and MHCII molecules in CD11c^{+} cells (Fig. 2f and g and Supplementary Fig. S4c). With the M13 phage as an efficient adjuvant, the efficiency of SIINFEKL peptide cross-presentation was enhanced about 61% compared with free OVA treatment (Fig. 2h and Supplementary Fig. S4d). Moreover, DCs maturation induced by M13 phage is mainly dependent on the Toll-like receptor (TLR) pathway activation based on the enrichment of CpG regions in the M13 phage genome [46]. CpG is a typical agonist for the TLR9 signaling pathway in DCs. As outlined in Fig. 2i and Supplementary Fig. S4e, the expression of TLR9 in BMDCs was increased significantly with M13, M13@PEI and MPO treatments. Additionally, there was no obvious activation effect of multiple TLRs (TLR3, TLR4, TLR7 and TLR8) related to the secretion of pro-inflammatory cytokines induced by MPO. However, the transcription abundances of TLR5 in MPO treated group was 1.66-folds higher than in M13 treated group account of the immunoadjuvant effect of PEI (an agonist of TLR5) (Supplementary Fig. S5a). Taken together, these results suggest that M13 phage-based vaccine can facilitate DC maturation and OVA antigen cross-presentation efficiently.

Macrophages (Macs) regarded as a kind of APCs play a pivotal role in regulating innate immunity [47]. M13 phage as a natural virus could awaken innate immune response by activating Macs. After co-cultured with various formulations and RAW 264.7 cells for 24 h, FCM was used for evaluation of Macs activation. Both M13 and MPO treatments obviously promoted the expression levels of CD86 in CD11b^{+} Macs (Fig. 2j). Prior studies have noted the importance of type I interferons (IFNs) in virus-related immune responses [48]. Therefore, we detected the transcriptional level of IFNs in Macs and DCs after being treated with M13 phage and MPO. When compared with the PBS group, it was apparent from Fig. 2k that the expression abundance of IFN-β and IFN-α was presented with a 2.4-fold and a 6-fold increase in Macs and DCs individually. Besides, various immunologic priming cytokines, tumor-necrosis factor-α (TNF-α), interferon-α (IFN-α), interleukin-6 (IL-6) and IL-12p40 secreted by BMDCs were determined by enzyme-linked immunosorbent assay (ELISA). In line with the DCs maturation assay, the M13 and MPO treatments induced a marked augmentation tendency of cytokines production (Fig. 2l).

Activation and proliferation of T cells are important for boosting tumor immune response strongly. It was interesting to note that phage could influence splenocyte proliferation activity [49]. We performed a co-cultured study of DCs and splenocytes for proliferation analysis, as assessed by 5-(6)-carboxyfluorescein diacetate succinimidyl diester (CFSE) dilution assay (Fig. 2m). Splenocytes were analyzed by FCM gating on CD8-positive T cells. As expected, DCs incubated with M13 phage and MPO induced significant proliferation of CD8^{+} T cells, and the proliferation rates improved about 88% and 89.5% compared with OVA treatment. These results demonstrate that M13 phage is supposed to be an adjuvant and vaccine vector platform with high efficiency for motivation of innate and adaptive immune responses.

3.2. in vitro CTL response and transcriptional analysis of the immune activation mechanism

We then investigated the antigen internalization of DCs by super-resolution confocal imaging. BMDCs were incubated with Cy5 labeled-OVA and MPO for 6 h. As shown in Fig. 3a and Supplementary Fig. S5a, the fluorescence intensity of the intracellular antigen in OVA-treated DCs was significantly weaker than that of the MPO treatment group. In addition, treatment DCs with the MPO vaccine resulted in an intension OVA red fluorescence overlapped with lysosome at 6 h account of the proton buffering capacity of PEI and adjuvants effect of M13 phage. After incubation for 24 h, an intense red fluorescence of OVA was observed on the DCs membrane. In contrast, fluorescent co-overlap of OVA and lysosome was found in free OVA treatment DCs, suggesting the antigen processing and cross-presentation more efficient with M13 phage vaccine treatment (Fig. 3b). The endocytosis antigen was also analyzed by FCM after co-incubation with Cy5 labeled-OVA and MPO for 24 h (Fig. 3c and Supplementary Fig. S5c). MPO treatment DCs showed the highest fluorescence intensity of OVA, approximately a 3.9-fold enhancement of the antigen uptake by comparison with the free OVA group.

To further explore the potency of the anti-tumor effects elicited by hybrid phage vaccine, *in vitro* specific cytotoxic T lymphocytes (CTL)-triggered tumor cell killing assay was conducted. Lactate dehydrogenase (LDH) release from the supernatant by dead tumor cells was detected to estimate the efficiency of T-cells mediated tumor cell killing effect (Fig. 3d). Apparently, MPO-treated splenocytes showed the strongest cytotoxicity toward B16-OVA cells. In contrast, M13 and M13@PEI treatments attenuated virulence due to the lack of antigen-specific immunity. The same result was also confirmed by IFN-γ secretion by splenocytes (Fig. 3e). Besides, there was a 29% increase in activated CD8^{+} T cells in the MPO treated group compared with the OVA treatment analyzed by FCM (Fig. 3f). Collectively, M13 phage-based vaccine displayed the ability to boost antigen-specific CTL response for tumor destruction efficaciously.
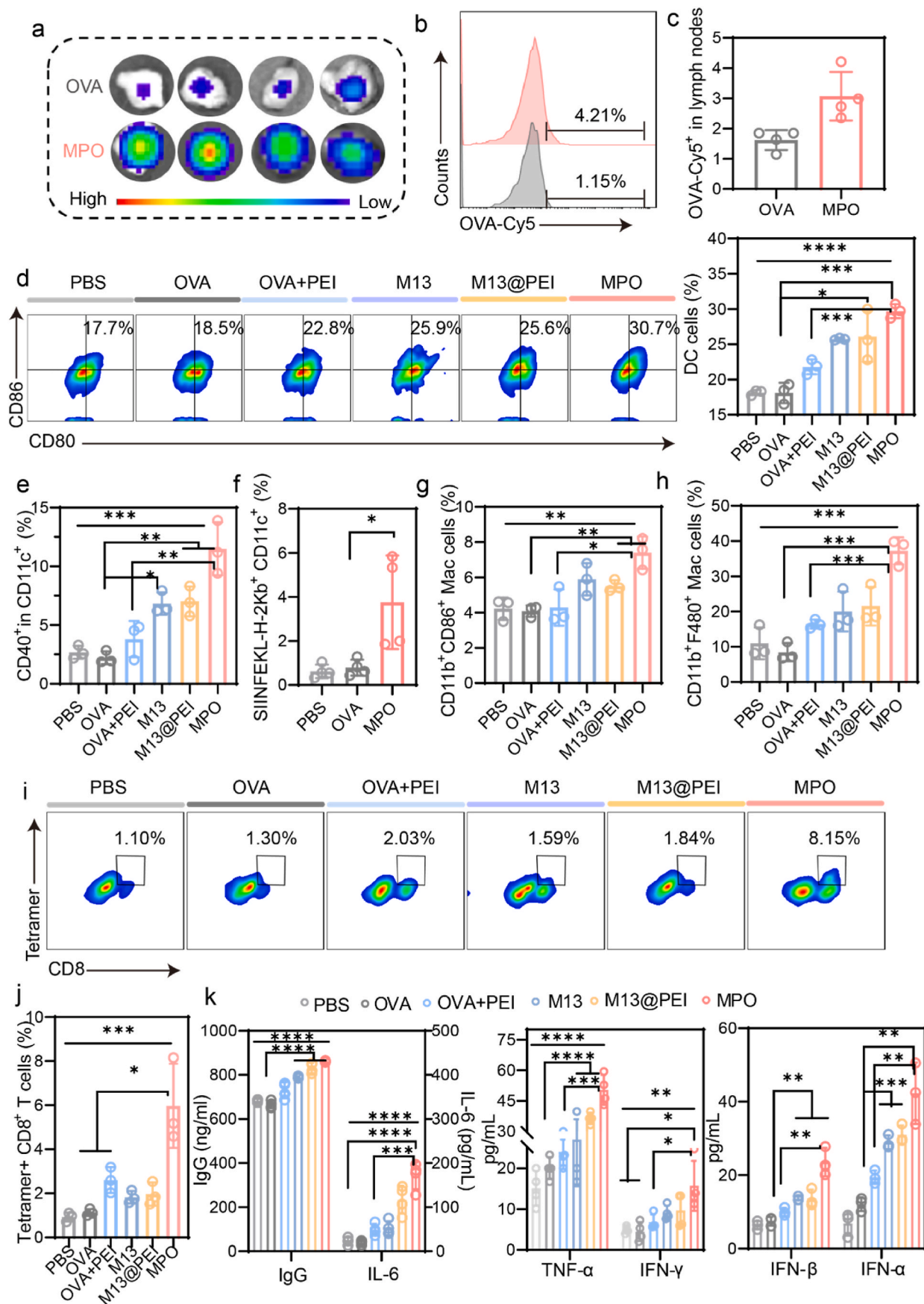
(caption on next page)

Fig. 4. Lymph node enrichment and *in vivo* immune activation. (a) The *ex vivo* fluorescence imaging of Cy5-labeled OVA in dLNs after injection of OVA and MPO at the tail base for 24 h (n = 4). (b–c) Representative FCM image (left) and corresponding quantification (right) of OVA uptake by CD11c$^+$ DCs in LNs after injection of OVA and MPO 24 h later (n = 4). (d) Typical FCM image (left) and statistical data (right) representing the up-regulation expression of CD80 and CD86 in CD11c$^+$ DCs on day 7 after vaccination various formulations (n = 3). (e) CD40-positive CD11c$^+$ DCs in dLNs with the same treatments as in panels d (n = 3). (f) Percentage of OVA (SIINFEKL)-presenting DCs in dLNs after OVA and MPO treatments for antigen presentation efficiency assessment (n = 3). (g–h) The proportion of activated macrophages with expression CD11b, CD86 and F4/80 in LNs after indicated treatments (n = 3). (i–j) Representative FCM image and corresponding quantification of the SIINFEKL tetramer staining of CD3$^+$CD8$^+$ T cells in PBMC. (k) Detection of various immune-associated cytokines content of IgG, TNF-α, IL-6, INF-γ, IFN-β and IFN-α in serum after different treatments 24 h later by ELISA assay (n = 4). Statistical significance was calculated with unpaired two-tailed Student's *t*-test and one-way ANOVA with Tukey post-hoc analysis. The mean values and S.D. are presented. *P < 0.05, **P < 0.01, ***P < 0.001, ****P < 0.0001.

To get a deeper understanding of the mechanisms of immune activation induced by M13 phage, the transcriptome of DCs was used for further analysis after treated with M13 phage for 24 h. As presented in Fig. 3g and Supplementary Figs. S6 and 119 up-regulated genes and 71 down-regulated genes expression associated with immune response in DCs treatment with M13 phage compared with PBS group were screened (fold change ≥2 and P < 0.05). Among these up-regulated genes were mainly immune activation positive-correlated, such as *Il6, Cd40, Cd80, Ifnb1* and *Irf7*. Kyoto Encyclopedia of Genes and Genomes (KEGG) was used to exhibit the major signaling pathway enrichment in DCs activation (Fig. 3h). For instance, cytokine-cytokine receptor interaction was engaged in innate as well as adaptive inflammatory host defenses. It was exhibited from the protein-protein interaction network in Fig. 3i, several kinds of functional protein networks involved in immunity were identified. These genes mainly affected the comprehensive immune activation effect of DCs by regulating inflammatory response, defense response, cytokine production and a series of immune responses, such as innate immune and adaptive immune. Such data provided a reasonable explanation for the specific mechanism of DCs activation caused by the M13 phage. From Genetic Ontology (GO) analysis, it was revealed that most genes referred to biological process, cellular component and molecular function were dramatically up-regulated expression in the M13 phage treated group (Supplementary Figs. S6b–c). Furthermore, a total 14,176 of genes were identified and shown in Venn diagram (Supplementary Fig. S6d), revealing the significant difference in transcripts between PBS and M13 treated group. Overall, these transcriptome results provide in-depth mechanisms analysis to investigate M13 phage-based APCs activation thoroughly.

3.3. The M13 phage-based vaccine for boosting immune response in vivo

To assess the enrichment of antigen in lymph nodes, Cy5-labeled OVA and MPO were subcutaneously injected at the tail base of C57BL/6 mice (Supplementary Fig. S7a). After 24 h, the draining lymph nodes (dLNs) and major organs were harvested for fluorescence imaging *ex vivo*. Compared to OVA treated group, MPO treatment showed a stronger fluorescence in dLNs. And there were no obvious fluorescence signals of Cy5-labeled OVA in major argans (Fig. 4a and Supplementary Figs. S7b–c). The same results were also confirmed by FCM (Fig. 4b-c). The M13 phage treatment resulted in a 47% increase in antigen internalization of DCs in the dLNs. These results collectively confirmed that M13 phage as an excellent immune adjuvant could effectively deliver antigens to dLNs.

Subsequently, we conducted *in vivo* immunological studies to evaluate the immune response provoked by the M13 phage vaccine. Mice were immunized with various formulations severally with equivalent doses of OVA and M13 phage. dLNs were collected and analyzed at 7 days post-injection. It was consistent with *in vitro* assays that OVA + PEI treated group showed a limited increase of the mature DCs compared with the OVA group (about 1.2-fold of enhancement). Meanwhile, the expression of mature DCs markers (CD11c, CD80, CD86 and CD40) was the highest in the MPO vaccination group among the treatments. Whereas, a slightly decreased proportion of mature DCs was detected in the M13 group, mainly because the virus resulted in clearance rapidly *in vivo* and disabled immunogenicity (Fig. 4d and e, Supplementary Fig. S8). Particularly, MPO treatment also improved the level of

SIINFEKL-H-2Kb peptide-cross presenting (about 78%) in dLNs in comparison to the OVA alone treated group (Fig. 4f and Supplementary Fig. S8). Furthermore, the number of activated Macs was also increased in dLNs after MPO immunization (Fig. 4g and h, Supplementary Figs. S8b–c), illustrating the strong innate immune response motivated by the MPO. Notably, the frequency of SIINFEKL-specific CD8$^+$ T cells of peripheral blood mononuclear cells (PBMCs) presented in a 5.28-fold, 2.3-fold increase in the MPO treated group compared with OVA alone group and OVA + PEI group, which suggested that the M13 phage-based vaccine could trigger the enhanced antigen-specific T-cell mediated immune responses (Fig. 4i and j). Mice serum were isolated after injection of indicated formulations 24 h later, and a series of cytokines were measured by ELISA assays (Fig. 4k). Levels of OVA-specific serum IgG were much higher in the MPO group than OVA alone treatment, which manifested the enhancement of OVA-specific response attributed to the M13 phage. Other cytokines containing TNF-α, IL-6, IFN-γ, IFN-β and IFN-α were totally showed the highest production in MPO immunized mice. Meanwhile, the highest levels of type I interferons including IFN-β and IFN-α were also observed in MPO treated group, which were 3.15-fold and 3.51-fold higher than the free OVA treated group. These results confirm that the M13 phage promotes antigen delivery to dLNs and evokes a robust immune effector process *in vivo*.

3.4. MPO vaccine for tumor prevention and suppression in the melanoma model

To assess the anti-tumor effect of MPO, we carried out *in vivo* studies on multiple melanoma models. We first evaluated the potential of MPO vaccine for tumor prevention. The healthy C57BL/6 mice were immunized subcutaneously with MPO and other control formulations once a week for a total of three times before the tumor transplantation (Fig. 5a). The tumor prevention efficiency was estimated by measuring tumor growth volume and recording the survival time of mice. The tumor growth was almost completely inhibited in MPO treated group in the first two weeks, and showed a certain increase trend latterly. By contrast, other treatments showed hardly any tumor prevention effects (Fig. 5b and Supplementary Fig. S9). On day 25, all mice in the PBS group died, but 83% of the mice that received MPO treatment were still alive (Fig. 5c). The proportion of memory T cells of PBMCs was detected after 42 days with vaccination (Fig. 5d). Both FCM images and quantification showed that there was about a 1.5-fold increase in effector memory T cells (T$_{EM}$) of MPO immunized mice compared with the PBS treated group.

Then, the therapeutic effect of MPO vaccine was conducted on the subcutaneous B16-OVA melanoma model (Fig. 5e). An immune checkpoint blockade (ICB), α-PD1, was selected to synergize with the MPO vaccine for strengthening the anti-tumor immune response. As exhibited in Fig. 5f and Supplementary Figs. S10a–b, MPO combination with α-PD1 treatment delayed tumor growth significantly compared with other treatments. However, the OVA + PEI treatment displayed a limited tumor inhibition effect. Meanwhile, tumor-infiltrating lymphocytes (TILs) were analyzed by FCM (Fig. 5g and h). The percentage of CD8$^+$ T cells in tumor tissues was improved 2.2- and 1.1-folds in MPO + α-PD1 treated group compared with OVA alone or MPO treatment severally. Together with immunohistochemical for Ki67 and immunofluorescence for IFN-γ, granzyme B and CD8 staining (Fig. 5i and
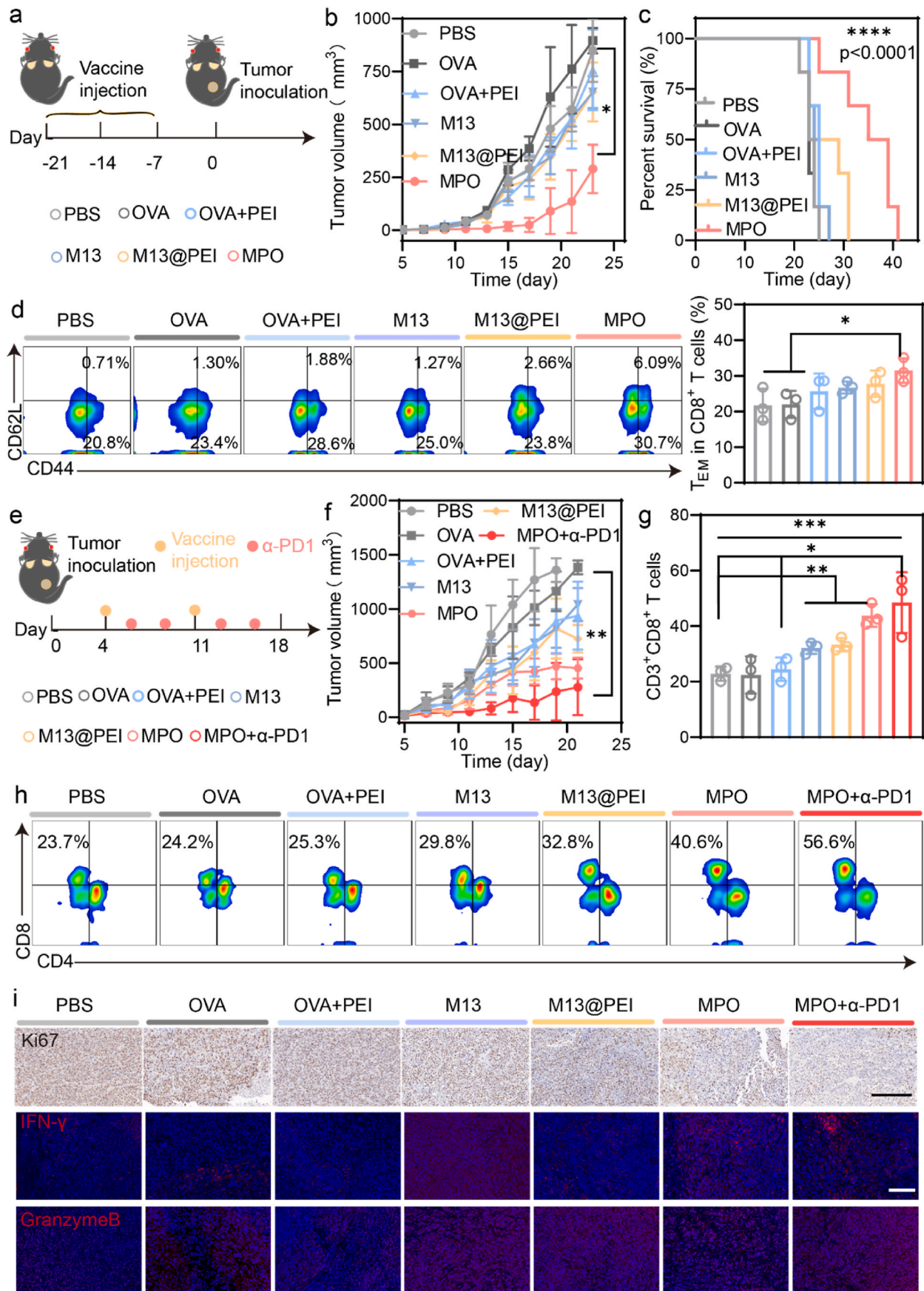
Fig. 5. MPO vaccine inhibits tumor growth in B16-OVA melanoma model. (a) Scheme of the prophylactic assay in vaccination and neoplasia. (b–c) Tumor growth and survival curves for prophylactic effect evaluation (n = 6). (d) Representative FCM image (left) and statistical data (right) of Tem cells (gated on CD8$^+$ T cells) in the peripheral blood on day 21 after inoculation B16-OVA cells (n = 3). (e) Timeline of anti-tumor treatments. (f) The anti-tumor therapeutic effect of MPO synergy ICB monitored by tumor growth curve (n = 6). (g–h) Quantitative analysis and FCM images of tumor-infiltrating CD8$^+$ T cells after indicated treatments on day 14 (n = 3). (i) Immunohistochemical staining of Ki67 and immunofluorescence of IFN-γ and Granzyme B for analysis tumor inhibition effect in tumor tissues (Scale bar: 200 μm). Statistical significance was calculated with unpaired two-tailed Student's *t*-test and one-way ANOVA with Tukey post-hoc analysis. The mean values and S. D. are presented. *P < 0.05, **P < 0.01, ***P < 0.001, ****P < 0.0001.

Supplementary Fig. S10c) proved that the MPO combined with ICB could trigger a powerful anti-tumor immune response. After that, the bio-safety assays of M13 phage were performed. It was noted from Supplementary Fig. S11 that there were almost no toxic side effects in major organs after M13 phage treatment. The blood biochemical and biochemical analysis also proved biocompatibility and security.

3.5. M13 phage-based platform for systemic immune response activation

To assess the systemic immune response triggered by the M13 phage-based vaccines, we also tested the anti-tumor metastasis effect induced by the MPO vaccine. C57BL/6 mice were injected intravenously with B16-OVA cells and then received different treatments 24 h later and the lung tissues were harvested on day 16 for further analysis (Fig. 6a). The MPO + α-PD1 treatment showed a substantial anti-metastasis effect, as evaluation by lung metastatic nodules (Fig. 6b), lung weight (Fig. 6c) and lung images (Supplementary Fig. S12). From H&E staining, MPO + α-PD1 treatment resulted in no obvious metastasis in the lung, whereas controls such as PBS, OVA and OVA + PEI group emerged in a large area of metastases (Fig. 6d). These results reveal that the MPO vaccine not only initiates the local immune of the tumor, also regulates the systemic immunity to eliminate tumor formation and metastasis.

Generally, resection is the main clinical treatment for cancers. However, tumor recurrence post-operation remains a challenge [50]. Using cell membrane-based vaccines is a promising strategy for tumor immune therapy [51,52]. Thus, Mem from primary tumors as antigens was collected and then fabricated with hybrid M13 phage to form MPM vaccine. We established a local tumor recurrence model for evaluation of autologous Mem-based personalized tumor immunotherapy (Fig. 6e). One week after inoculation of the tumor cells (4T1-luc), mice were surgically excised tumors to collect tumor tissues and separate autologous cell membranes. Mice were immunized with various formulations as indicated on day 4 post-surgery (Supplementary Fig. S13a). Tumor recurrence was tracked by *in vivo* bioluminescence imaging once a week. The local recurrence in the PBS group was clearly observed. By contrast, mice immunized with MPM showed weak bioluminescence intensity. Especially, α-PD1 combination therapy dramatically facilitated the anti-tumor effect of MPM (Fig. 6f and Supplementary Figs. S13b–c). In the MPM and MPM + α-PD1 group, 67% (4 of the 6 mice) and 83% (5 of the 6 mice) of the mice survived longer than 60 days respectively (Fig. 6g).

To further explore the immune memory effects motivated by MPM vaccine-based ICB combination therapy, PBMCs were isolated to analyze the levels of CD8$^+$ memory T cells on day 60. Mice in the PBS group were 60 days old healthy mice. The quantitative and FCM analyses revealed that the percentage of central memory T cells (T$_{CM}$) and TEM gated on CD8$^+$ T cells was significantly higher than the untreated group in expectation, which were 1.6-fold and 2.5-fold increase correspondingly (Fig. 6h and i). Moreover, MPM + α-PD1 treatment could strengthen the immune memory response with the enhanced serum cytokines of TNF-α and IFN-γ secretion (Fig. 6j).

According to the above *in vivo* anti-tumor assays, the powerful immunomodulatory ability of M13 phage vaccine was evidenced. Here, we aim to develop an antigen delivery platform based on M13 hybrid phage for the application of multiple tumor model adaptability. A clinically relevant orthotopic breast tumor model was established (Supplementary Fig. S14a). MPM combination with α-PD1 showed a promising therapeutic effect (Supplementary Figs. S14b–c). Within 50

days after MPM + α-PD1 treatment, the survival rate of mice was as high as 67% (4 of the 6 mice) (Supplementary Fig. S14d). Moreover, based on our previous work [53], we constructed two neoantigen cell lines of breast cancer (4T1^{neo}) and colorectal cancer (CT26^{neo}) by knockout *Mlh1* to further evaluate the anti-tumor effect of M13 phage-based vaccine. As shown in Supplementary Fig. S15a-c, MPM combination α-PD1 group showed an approximately 88% tumor-inhibition rate at the end of the treatment. In addition, the proportion of CD8$^+$ T cells in TILs after treated with MPM + α-PD1 was much higher than in other groups, and 5.1-fold CD3$^+$ CD8$^+$ T cells were increased compared with the PBS group (Supplementary Fig. S15d). The immunohistochemical and immunofluorescence staining collectively illustrated that MPM vaccine synergy with ICB could elicit a robust neoantigen-specific immune response (Supplementary Fig. S16). The same results were also verified in the colorectal cancer (CT26^{neo}) model (Supplementary Figs. S17–S18).

4. Conclusion

In sum, we proposed a novel strategy to design cancer vaccine platform based on hybrid M13 phage (M13@PEI) for personalized immunotherapy. Such hybrid phage-based vaccine (HMP@Ag) exhibited a high-efficiency adjuvant effect of APCs activation and antigen cross-presentation. Besides, M13@PEI as a distinct vector could promote antigens (peptide, protein and cell membrane) delivery into dLNs and elicit a strong T cell-mediated anti-tumor response. Multiple *in vivo* studies revealed that the HMP@Ag combination ICB therapy could further amplify the immunological effect induced by HMP@Ag. As displayed in melanoma model and orthotopic breast cancer, HMP@Ag vaccine plus α-PD1 showed excellent capacity for primary and metastatic tumors elimination. The specific neoantigen-based immune response was also demonstrated in two kinds of subcutaneous neoantigen-based models after receiving MPM + α-PD1 treatment. What's more, in a clinically relevant post-operation recurrence of cancer model, the therapeutics of personalized immunotherapy based on MPM vaccine tailored with autologous cell membrane was confirmed synergy with α-PD1 highly efficiency. Notably, it was certified that when combined with the ICB of α-PD1, MPM could stimulate the host immune system to generate a durable immune-memory effect. Due to the lack of specificity of TAAs, such personalized cancer vaccines customized by individuals might have great potential for clinical translation.

Emerging tumor immunotherapy presents a new opportunity for the future. Reasonable modification and design for natural active materials, like viruses with high immunogenicity are conclusively for cancer vaccine development. This work has successfully indicated that the hybrid M13 phage-based vaccine platform could boost potent anti-tumor response. We highlight the importance of a personalized vaccine vector integrating innate and adaptive immunity by using biosafety active materials. We anticipate that such a hybrid M13 phage-based vaccine platform may provide an insight to exploit natural adjuvant or carrier for vaccine design with enhanced efficiency. More broadly, this platform may be extended to other immune-related disease treatments, such as bacterial infections.

Credit author statement

X.D. and X.Z.Z. conceived the project and designed the experiments. X.D., P.P. synthesized materials. X.D. and J.J.Y performed *in vitro* cell
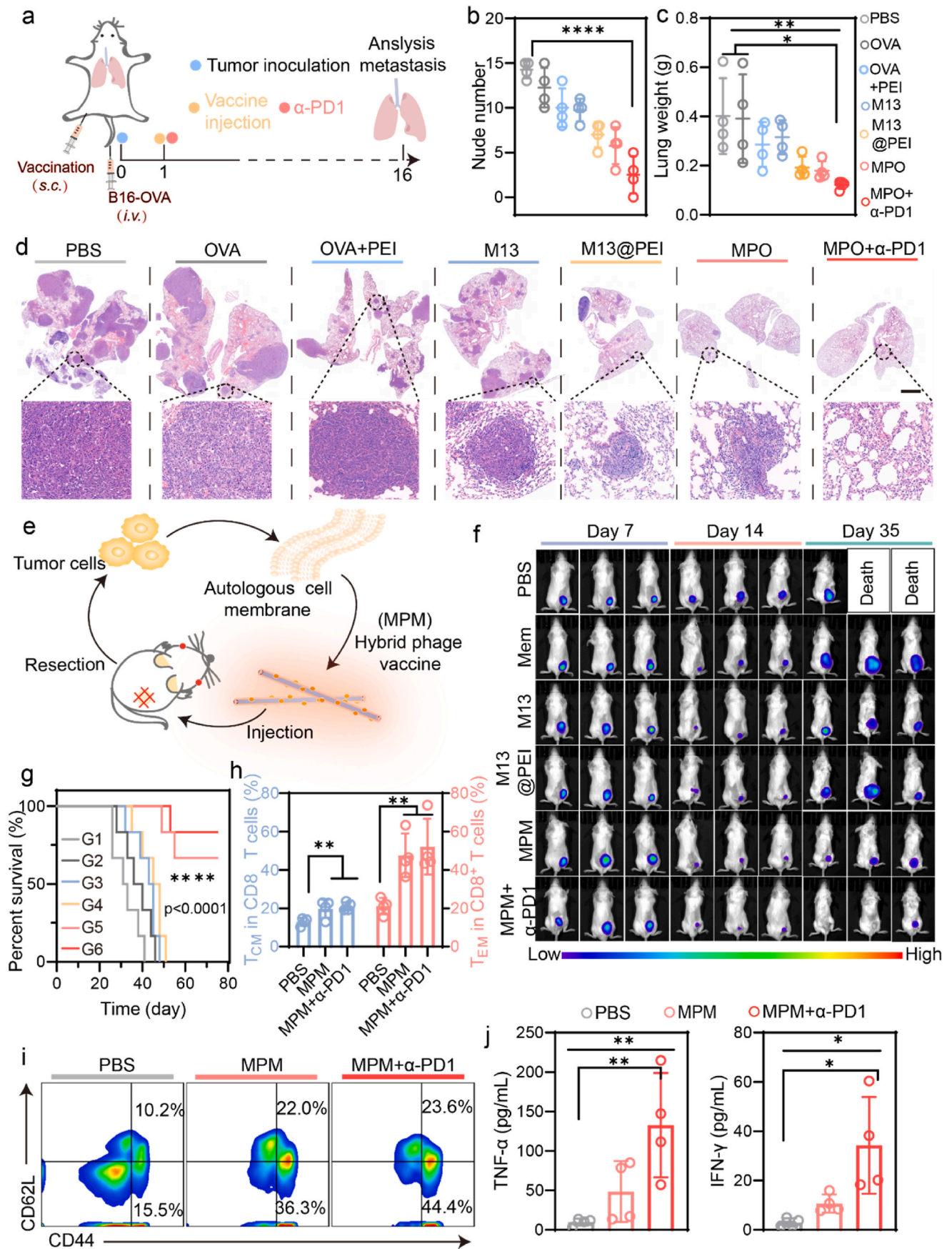
(caption on next page)

Fig. 6. HMP@Ag platforms for triggering systemic immunity to suppress tumor metastasis and recurrence. (a) Scheme of the model construction and treatment of lung metastasis. (b–c) The statistical data of the nodules and weight in the lungs. After injection (*i.v.*) of B16-OVA cells, mice were vaccinated with various formulations. The lungs were harvested after 16 days to image and analyze. (d) The H&E staining of lungs collected from various treatments of mice for tumor metastases evaluation (Scale bar: 1 mm). (e) Schematic for illustration the process of personalized autologous-based vaccine preparation after post-surgery. (f) *In vivo* bioluminescence images for monitoring recurrence of breast cancer (n = 6). The primary tumors resection and vaccination were conducted on day 7 and day 11, separately. (g) Survival curve of recurrence breast cancer with various treatments. (h–i) Proportion of TCM and TEM in j and typical FCM image in k in the peripheral blood of recurrence model mice on day 60 after receiving the same treatments as in panels h (n = 4). (j) Detection cytokines of TNF-α (left) and IFN-γ (right) levels in serum of recurrence model mice on day 60 (n = 4). G1: PBS; G2: Mem; G3: M13; G4: M13@PEI; G5: MPM; G6: MPM + α-PD1. Statistical significance between the two groups was determined by two-sided unpaired t-tests, and multi-group comparison was calculated one-way ANOVA with Tukey post-hoc analysis. The mean values and S.D. are presented. *P < 0.05, **P < 0.01, ***P < 0.001, ****P < 0.0001.

experiments. X.D., P.P. and J.J.Y. performed *in vivo* experiments. X.D., P. P. and Q.L.Z. collected and analyzed the data. X.D., P.P. and Q.L.Z. and X.Z.Z. co-wrote the manuscript. All authors discussed the results and reviewed the manuscript.

Declaration of competing interest

The authors declare that they have no known competing financial interests or personal relationships that could have appeared to influence the work reported in this paper.

Data availability

Data will be made available on request.

Appendix B. Supplementary data

Supplementary data to this article can be found online at https://doi. org/10.1016/j.biomaterials.2022.121763.

References

[1] W. Jiang, Y. Wang, J.A. Wargo, F.F. Lang, B.Y.S. Kim, Considerations for designing preclinical cancer immune nanomedicine studies, Nat. Nanotechnol. 16 (2021) 6–15.

[2] H. Wang, A.J. Najibi, M.C. Sobral, B.R. Seo, J.Y. Lee, D. Wu, A.W. Li, C.S. Verbeke, D.J. Mooney, Biomaterial-based scaffold for in situ chemo-immunotherapy to treat poorly immunogenic tumors, Nat. Commun. 11 (2020) 5696.

[3] A. Harari, M. Graciotti, M. Bassani-Sternberg, L.E. Kandalaft, Antitumour dendritic cell vaccination in a priming and boosting approach, Nat. Rev. Drug Discov. 19 (2020) 635–652.

[4] J.D. Martin, H. Cabral, T. Stylianopoulos, R.K. Jain, Improving cancer immunotherapy using nanomedicines: progress, opportunities and challenges, Nat. Rev. Clin. Oncol. 17 (2020) 251–266.

[5] L. Tian, Y. Zhu, J. Xu, M. Shao, W. Zhu, Z. Xiao, Q. Chen, Z. Liu, Coordination polymers integrating metalloimmunology with immune modulation to elicit robust cancer chemoimmunotherapy, CCS Chem 3 (2021) 2629–2642.

[6] E.A. Gosselin, H.B. Eppler, J.S. Bromberg, C.M. Jewell, Designing natural and synthetic immune tissues, Nat. Mater. 17 (2018) 484–498.

[7] M. Saxena, S.H. van der Burg, C.J.M. Melief, N. Bhardwaj, Therapeutic cancer vaccines, Nat. Rev. Cancer 21 (2021) 360–378.

[8] Q. Fan, Q. Ma, J. Bai, J. Xu, Z. Fei, Z. Dong, A. Maruyama, K.W. Leong, Z. Liu, C. Wang, An implantable blood clot-based immune niche for enhanced cancer vaccination, Sci. Adv. 6 (2020), eabb4639.

[9] X. Xi, T. Ye, S. Wang, X. Na, J. Wang, S. Qing, X. Gao, C. Wang, F. Li, W. Wei, G. Ma, Self-healing microcapsules synergetically modulate immunization microenvironments for potent cancer vaccination, Sci. Adv. 6 (2020), eaay7735.

[10] R. Kuai, L.J. Ochyl, K.S. Bahjat, A. Schwendeman, J.J. Moon, Designer vaccine nanodiscs for personalized cancer immunotherapy, Nat. Mater. 16 (2017) 489–496.

[11] A.W. Li, M.C. Sobral, S. Badrinath, Y. Choi, A. Graveline, A.G. Stafford, J. C. Weaver, M.O. Dellacherie, T.Y. Shih, O.A. Ali, J. Kim, K.W. Wucherpfennig, D. J. Mooney, A facile approach to enhance antigen response for personalized cancer vaccination, Nat. Mater. 17 (2018) 528–534.

[12] X. Li, X. Wang, A. Ito, N.M. Tsuji, A nanoscale metal organic frameworks-based vaccine synergises with PD-1 blockade to potentiate anti-tumour immunity, Nat. Commun. 11 (2020) 3858.

[13] J.J. Moon, H. Suh, A. Bershteyn, M.T. Stephan, H. Liu, B. Huang, M. Sohail, S. Luo, S.H. Um, H. Khant, J.T. Goodwin, J. Ramos, W. Chiu, D.J. Irvine, Interbilayer-crosslinked multilamellar vesicles as synthetic vaccines for potent humoral and cellular immune responses, Nat. Mater. 10 (2011) 243–251.

[14] L. Wei, Y. Zhao, X. Hu, L. Tang, Redox-responsive polycondensate neoepitope for enhanced personalized cancer vaccine, ACS Cent. Sci. 6 (2020) 404–412.

[15] Y. Wang, S. Lin, H. Jiang, Y. Gu, Y. Wu, J. Ma, Y. Ke, L.W. Zhang, Y. Wang, M. Gao, Visualizable delivery of nanodisc antigen-conjugated adjuvant for cancer immunotherapy, C. C. S. Chemistry (2021) 1328–1340.

[16] S. Liu, Q. Jiang, X. Zhao, R. Zhao, Y. Wang, Y. Wang, J. Liu, Y. Shang, S. Zhao, T. Wu, Y. Zhang, G. Nie, B. Ding, A DNA nanodevice-based vaccine for cancer immunotherapy, Nat. Mater. 20 (2021) 421–430.

[17] J. Koerner, D. Horvath, V.L. Herrmann, A. MacKerracher, B. Gander, H. Yagita, J. Rohayem, M. Groettrup, PLGA-particle vaccine carrying TLR3/RIG-I ligand Riboxxim synergizes with immune checkpoint blockade for effective anti-cancer immunotherapy, Nat. Commun. 12 (2021) 2935.

[18] H. Qin, R. Zhao, Y. Qin, J. Zhu, L. Chen, C. Di, X. Han, K. Cheng, Y. Zhang, Y. Zhao, J. Shi, G.J. Anderson, Y. Zhao, G. Nie, Development of a cancer vaccine using in vivo click-chemistry-mediated active lymph node accumulation for improved immunotherapy, Adv. Mater. 33 (2021), e2006007.

[19] N. Gong, Y. Zhang, X. Teng, Y. Wang, S. Huo, G. Qing, Q. Ni, X. Li, J. Wang, X. Ye, T. Zhang, S. Chen, Y. Wang, J. Yu, P.C. Wang, Y. Gan, J. Zhang, M.J. Mitchell, J. Li, X.J. Liang, Proton-driven transformable nanovaccine for cancer immunotherapy, Nat. Nanotechnol. 15 (2020) 1053–1064.

[20] Z. Hu, P.A. Ott, C.J. Wu, Towards personalized, tumour-specific, therapeutic vaccines for cancer, Nat. Rev. Immunol. 18 (2018) 168–182.

[21] D.J. Irvine, M.A. Swartz, G.L. Szeto, Engineering synthetic vaccines using cues from natural immunity, Nat. Mater. 12 (2013) 978–990.

[22] D. Lee, K. Huntoon, Y. Wang, W. Jiang, B.Y.S. Kim, Harnessing innate immunity using biomaterials for cancer immunotherapy, Adv. Mater. 33 (2021), e2007576.

[23] H. Pan, M. Zheng, A. Ma, L. Liu, L. Cai, Cell/bacteria-based bioactive materials for cancer immune modulation and precision therapy, Adv. Mater. (2021), e2100241.

[24] B. Pulendran, S.A. P, D.T. O'Hagan, Emerging concepts in the science of vaccine adjuvants, Nat. Rev. Drug Discov. 20 (2021) 454–475.

[25] D.J. Lynn, S.C. Benson, M.A. Lynn, B. Pulendran, Modulation of immune responses to vaccination by the microbiota: implications and potential mechanisms, Nat. Rev. Immunol. 22 (2021) 33–46, https://doi.org/10.1038/s41577-021-00554-7.

[26] A.D. Waldman, J.M. Fritz, M.J. Lenardo, A guide to cancer immunotherapy: from T cell basic science to clinical practice, Nat. Rev. Immunol. 20 (2020) 651–668.

[27] L. Chen, H. Qin, R. Zhao, X. Zhao, L. Lin, Y. Chen, Y. Lin, Y. Li, Y. Qin, Y. Li, S. Liu, K. Cheng, H. Chen, J. Shi, G.J. Anderson, Y. Wu, Y. Zhao, G. Nie, Bacterial cytoplasmic membranes synergistically enhance the antitumor activity of autologous cancer vaccines, Sci. Transl. Med. 13 (2021), eabc2816.

[28] C.R. Gurbatri, I. Lia, R. Vincent, C. Coker, S. Castro, P.M. Treuting, T.E. Hinchliffe, N. Arpaia, T. Danino, Engineered probiotics for local tumor delivery of checkpoint blockade nanobodies, Sci. Transl. Med. 12 (2020), eaax0876.

[29] D.G. Roy, K. Geoffroy, M. Marguerie, S.T. Khan, N.T. Martin, J. Kmiecik, D. Bobbala, A.S. Aitken, C.T. de Souza, A.B. Stephenson, B.D. Lichty, R.C. Auer, D. F. Stojdl, J.C. Bell, M.C. Bourgeois-Daigneault, Adjuvant oncolytic virotherapy for personalized anti-cancer vaccination, Nat. Commun. 12 (2021) 2626.

[30] M. Super, E.J. Doherty, M.J. Cartwright, B.T. Seiler, F. Langellotto, N. Dimitrakakis, D.A. White, A.G. Stafford, M. Karkada, A.R. Graveline, C. L. Horgan, K.R. Lightbown, F.R. Urena, C.D. Yeager, S.A. Rifai, M.O. Dellacherie, A. W. Li, C. Leese-Thompson, H. Ijaz, A.R. Jiang, V. Chandrasekhar, J.M. Scott, S. L. Lightbown, D.E. Ingber, D.J. Mooney, Biomaterial vaccines capturing pathogen-associated molecular patterns protect against bacterial infections and septic shock, Nat. Biomed. Eng. 6 (2021) 8–18, https://doi.org/10.1038/s41551-021-00756-3.

[31] K. Esfahani, A. Elkrief, C. Calabrese, R. Lapointe, M. Hudson, B. Routy, W. H. Miller Jr., L. Calabrese, Moving towards personalized treatments of immune-related adverse events, Nat. Rev. Clin. Oncol. 17 (2020) 504–515.

[32] H. Huh, S. Wong, J. St Jean, R. Slavcev, Bacteriophage interactions with mammalian tissue: therapeutic applications, Adv. Drug Deliv. Rev. 145 (2019) 4–17.

[33] H.Y. Wang, Y.C. Chang, C.W. Hu, C.Y. Kao, Y.A. Yu, S.K. Lim, K.Y. Mou, Development of a novel cytokine vehicle using filamentous phage display for colorectal cancer treatment, ACS Synth. Biol. 10 (2021) 2087–2095.

[34] C.J. Desmet, K.J. Ishii, Nucleic acid sensing at the interface between innate and adaptive immunity in vaccination, Nat. Rev. Immunol. 12 (2012) 479–491.

[35] P. Tao, J. Zhu, M. Mahalingam, H. Batra, V.B. Rao, Bacteriophage T4 nanoparticles for vaccine delivery against infectious diseases, Adv. Drug Deliv. Rev. 145 (2019) 57–72.

[36] X. Dong, P. Pan, D.-W. Zheng, P. Bao, X. Zeng, X.-Z. Zhang, Bioinorganic hybrid bacteriophage for modulation of intestinal microbiota to remodel tumor-immune microenvironment against colorectal cancer, Sci. Adv. 6 (2020), eaba1590.

[37] L. D'Apice, V. Costa, R. Sartorius, M. Trovato, M. Aprile, P. De Berardinis, Stimulation of innate and adaptive immunity by using filamentous bacteriophage fd targeted to DEC-205, J. Immunol. Res. 2015 (2015), 585078.

[38] M. Karimi, H. Mirshekari, S.M. Moosavi Basri, S. Bahrami, M. Moghoofei, M. R. Hamblin, Bacteriophages and phage-inspired nanocarriers for targeted delivery of therapeutic cargos, Adv. Drug Deliv. Rev. 106 (2016) 45–62.

[39] Q. Bao, X. Li, G. Han, Y. Zhu, C. Mao, M. Yang, Phage-based vaccines, Adv. Drug Deliv. Rev. 145 (2019) 40–56.

[40] G.R. Souza, J.R. Molina, R.M. Raphael, M.G. Ozawa, D.J. Stark, C.S. Levin, L. F. Bronk, J.S. Ananta, J. Mandelin, M.M. Georgescu, J.A. Bankson, J.G. Gelovani, T.C. Killian, W. Arap, R. Pasqualini, Three-dimensional tissue culture based on magnetic cell levitation, Nat. Nanotechnol. 5 (2010) 291–296.

[41] Y. Choi, S.Y. Lee, Biosynthesis of inorganic nanomaterials using microbial cells and bacteriophages, Nat. Rev. Chem 4 (2020) 638–656.

[42] A. Shahrivarkevishahi, M.A. Luzuriaga, F.C. Herbert, A.C. Tumac, O.R. Brohlin, Y. H. Wijesundara, A.V. Adlooru, C. Benjamin, H. Lee, P. Parsamian, J. Gadhvi, N. J. De Nisco, J.J. Gassensmith, PhotothermalPhage: a virus-based photothermal therapeutic agent, J. Am. Chem. Soc. 143 (2021) 16428–16438.

[43] K.S. Sunderland, M. Yang, C. Mao, Phage-enabled nanomedicine: from probes to therapeutics in precision medicine, Angew. Chem. Int. Ed. 56 (2017) 1964–1992.

[44] J. Xu, J. Lv, Q. Zhuang, Z. Yang, Z. Cao, L. Xu, P. Pei, C. Wang, H. Wu, Z. Dong, Y. Chao, C. Wang, K. Yang, R. Peng, Y. Cheng, Z. Liu, A general strategy towards personalized nanovaccines based on fluoropolymers for post-surgical cancer immunotherapy, Nat. Nanotechnol. 15 (2020) 1043–1052.

[45] K. Cheng, R. Zhao, Y. Li, Y. Qi, Y. Wang, Y. Zhang, H. Qin, Y. Qin, L. Chen, C. Li, J. Liang, Y. Li, J. Xu, X. Han, G.J. Anderson, J. Shi, L. Ren, X. Zhao, G. Nie, Bioengineered bacteria-derived outer membrane vesicles as a versatile antigen display platform for tumor vaccination via Plug-and-Display technology, Nat. Commun. 12 (2021) 2041.

[46] R. Jamaledin, R. Sartorius, C. Di Natale, R. Vecchione, P. De Berardinis, P.A. Netti, Recombinant filamentous bacteriophages encapsulated in biodegradable polymeric microparticles for stimulation of innate and adaptive immune responses, Microorganisms 8 (2020).

[47] P. Roy, M. Orecchioni, K. Ley, How the immune system shapes atherosclerosis: roles of innate and adaptive immunity, Nat. Rev. Immunol. 22 (2021) 251–265, https://doi.org/10.1038/s41577-021-00584-1.

[48] L. Zitvogel, L. Galluzzi, O. Kepp, M.J. Smyth, G. Kroemer, Type I interferons in anticancer immunity, Nat. Rev. Immunol. 15 (2015) 405–414.

[49] M. Zimecki, B. Weber-Dabrowska, M. Lusiak-Szelachowska, M. Mulczyk, J. Boratynski, G. Pozniak, D. Syper, A. Górski, Bacteriophages provide regulatory signals in mitogen-induced murine splenocyte proliferation, Cell. Mol. Biol. Lett. 8 (2003) 699–712.

[50] Q. Chen, C. Wang, X. Zhang, G. Chen, Q. Hu, H. Li, J. Wang, D. Wen, Y. Zhang, Y. Lu, G. Yang, C. Jiang, J. Wang, G. Dotti, Z. Gu, In situ sprayed bioresponsive immunotherapeutic gel for post-surgical cancer treatment, Nat. Nanotechnol. 14 (2019) 89–97.

[51] W.L. Liu, M.Z. Zou, T. Liu, J.Y. Zeng, X. Li, W.Y. Yu, C.X. Li, J.J. Ye, W. Song, J. Feng, X.Z. Zhang, Cytomembrane nanovaccines show therapeutic effects by mimicking tumor cells and antigen presenting cells, Nat. Commun. 10 (2019) 3199.

[52] L. Sun, Z. Xiong, F. Shen, Z. Wang, Z. Liu, Biological membrane derived nanomedicines for cancer therapy, Sci. China Chem. 64 (2021) 719–733.

[53] D.W. Zheng, F. Gao, Q. Cheng, P. Bao, X. Dong, J.X. Fan, W. Song, X. Zeng, S. X. Cheng, X.Z. Zhang, A vaccine-based nanosystem for initiating innate immunity and improving tumor immunotherapy, Nat. Commun. 11 (2020) 1985.